AIP | Applied Physics Letters

The morphology of graphene on a non-developable concave substrate

Yuli Chen, Yong Ma, Shengtao Wang, Yanguang Zhou, and Hao Liu

Citation: Applied Physics Letters **108**, 031905 (2016); doi: 10.1063/1.4940232
View online: http://dx.doi.org/10.1063/1.4940232
View Table of Contents: http://scitation.aip.org/content/aip/journal/apl/108/3?ver=pdfcov
Published by the AIP Publishing

The morphology of graphene on a non-developable concave substrate

Yuli Chen,[1,a)] Yong Ma,[1] Shengtao Wang,[1] Yanguang Zhou,[2,3] and Hao Liu[1]
[1]*Institute of Solid Mechanics, Beihang University (BUAA), Beijing 100191, People's Republic of China*
[2]*Institute of Mineral Engineering, Division of Materials Science and Engineering, Faculty of Georesources and Materials Engineering, RWTH Aachen University, 52064 Aachen, Germany*
[3]*Aachen Institute for Advanced Study in Computational Engineering Science (AICES), RWTH Aachen University, 52062 Aachen, Germany*

(Received 22 October 2015; accepted 7 January 2016; published online 21 January 2016)

The performances of graphene sheet in micro- and nano-electronics and devices are significantly affected by its morphology, which depends on the surface features of the supporting substrate. The substrates with non-developable concave surface are widely used with graphene sheet in applications but rarely studied. Therefore, a theoretical model is established based on the energy analysis to explain the adhesion mechanisms and predict the morphology of the graphene sheet on a non-developable concave surface. Four different morphologies of the graphene sheet are revealed, and the critical conditions are established to predict which morphology the graphene/substrate system belongs to. For the monolayer graphene sheets much larger than the concave of substrate, the final equilibrium morphology is dominated by the half cone angle of the concave. The graphene sheet conforms completely to the SiO_2 substrate if the half cone angle is less than 27.5° and spans over the concave if the angel is larger than 27.5°. For graphene sheets smaller than the concave, they fall into the concave and the final morphology depends only on the ratio of graphene radius to concave radius. The monolayer graphene sheet conforms to the concave if the radius ratio is less than 0.51 and wrinkles if the ratio is larger than 0.51. The theoretical results are verified by a series of molecular dynamics simulations on various graphene/substrate systems. This work can provide guidelines to design high quality graphene-coated functional materials and devices, and can offer criterion for graphene-derived nano-electronics and nano-sensors. © *2016 AIP Publishing LLC*.
[http://dx.doi.org/10.1063/1.4940232]

Graphene displays remarkable electronic,[1–3] optical,[4] thermal,[5] and mechanical[6] properties due to its unique two-dimensional (2D) honeycomb structure and therefore has great promise for use in nano-electronics,[7,8] nano-devices,[9,10] and supercapacitors.[11] Recent studies show that these properties are strongly tied to the morphology of graphene.[12–14] For instance, random wrinkles, corrugations, and exfoliations of graphene lead to unpredictable electronic properties, which is fatal for nano electronic devices.[12,15]

In practical applications, graphene is always attached to a substrate to suppress the intrinsic random ripples in freestanding graphene sheet.[16] The surface features of substrate affect the graphene morphology significantly.[17–19] Therefore, it is of great importance to study the morphology of graphene sheet on substrate. Some studies have been carried out on the morphology of substrate-supported graphene sheets. However, most of them focus on the developable surfaces,[20–23] such as sinusoidal grooves surface,[21] and only a few studies are conducted for the undevelopable surface.[24] In fact, the non-developable surfaces,[25,26] especially the non-developable concave surfaces, are more common in applications. For example, non-developable cavities are common microstructures in some special optical instruments,[27] the molds for precision glass optics,[28] and the photovoltaic film devices.[29] In these applications, graphene is widely used as protective coatings and/or transparent conducting layers, and thus required to cover the target substrates completely and uniformly. However, a criterion to judge whether or not the graphene sheet can conform to a substrate with concave dents still remains to be established.

The purpose of this letter is to build an analytic mechanics model to explain the adhesive mechanisms of the graphene sheet on a non-developable concave surface and to predict the morphology of the graphene sheet. The continuum theory is adopted to analyze the morphology of graphene and the results are verified by molecular dynamics (MD) simulations. This study will provide the critical conditions to predict the morphologies of substrate-supported graphene sheets, which could be applied as guidelines to the nanostructure design and the graphene morphology control.

Fig. 1 presents a system with a round monolayer graphene sheet and a substrate with a concave of inverted spherical cap. The radius of the graphene sheet is r_g, and the radius and the half cone angle of the spherical cap are R_s and ω_s, respectively, as shown in Fig. 1(b). The graphene sheet may completely or partially conform to the substrate due to the adhesive interactions between the sheet and the substrate, and the final equilibrium morphology is determined by the minimum energy of the system. Four possible types of final graphene morphology may appear in the graphene/substrate systems with various graphene radius r_g, substrate concave radius R_s, and half cone angle ω_s. As illustrated in Figs. 2(a)–2(d), the graphene sheet can either (a) fully conform to the substrate or (b) span over the substrate if it is large enough. Otherwise, if the area of graphene sheet is smaller

[a)]Author to whom correspondence should be addressed. Electronic mail: yulichen@buaa.edu.cn

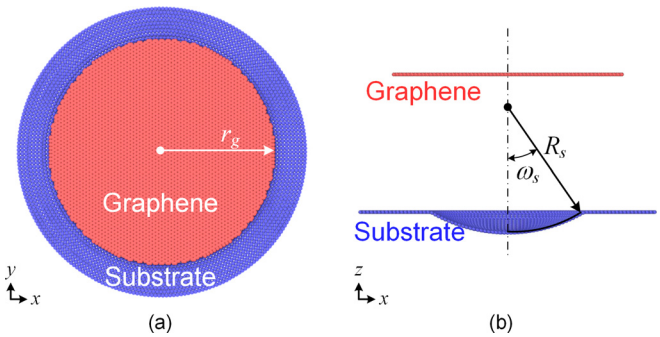

FIG. 1. The schematic of graphene and concave substrate: (a) top view and (b) side view.

than or nearly as large as the surface area of the concave, the sheet falls into the concave, and either (c) conforms to the concave or (d) wrinkles. Generally, the graphene sheet is much larger than the concave, so this letter will first focus on types (a) and (b) and then discuss types (c) and (d) briefly.

Fig. 2(e) presents the theoretical axisymmetric model for types (a) and (b), in which the graphene sheet is divided into three regions: (I) floating region, (II) curving region, and (III) annulus region. The final morphology of graphene can be described uniquely by the half cone angle $\omega_{(I)}$ of the floating region. The half cone angle $\omega_{(I)} > 0$ means that the sheet spans over the concave substrate, i.e., type (b) of the morphology, and $\omega_{(I)} = 0$ indicates that the sheet completely conforms to the substrate, i.e., type (a) of the morphology.

An energy-based analysis is carried out to establish the critical condition to judge whether a monolayer graphene sheet can completely conform to the inverted spherical cap. The total system energy E_T consists of three parts: the membrane energy E_m due to the in-plane deformation of graphene, the bending energy E_b due to the bending deformation of graphene, and the adhesion energy E_{ad} due to the interactions between graphene and substrate. The strain energy in the substrate is ignored because the substrate is much thicker than the graphene and thus the deformation is constrained by the lower-layer material.[24]

The membrane energy can be expressed as

$$E_m = \int_{A_g} \frac{Et}{2(1-\nu^2)} \left(\varepsilon_r^2 + 2\nu\varepsilon_r\varepsilon_\varphi + \varepsilon_\varphi^2\right) \mathrm{d}A_g, \tag{1}$$

where E, ν, t, and A_g are the Young's modulus, Poisson's ratio, thickness, and area of graphene, respectively. In this study, $Et = 275\,\mathrm{N/m}$ (Refs. 30 and 31) and $\nu = 0.186$ (Refs. 32 and 33) are adopted. ε_r and ε_φ are the radial and hoop strains of the graphene.

Assume that the flat graphene first goes through a planar uniform hydrostatic tension and then a simple hoop deformation to form its final morphology. Accordingly, the radial strain ε_r in regions I and II is a constant, denoted by $\varepsilon_{r(\mathrm{I})} = \varepsilon_{r(\mathrm{II})} = \varepsilon_0$, and the radii of regions I and II are $r_{(\mathrm{I})} = R_g \sin\omega_{(\mathrm{I})}/(1+\varepsilon_0)$ and $r_{(\mathrm{II})} = R_g(\omega_s - \omega_{(\mathrm{I})} + \sin\omega_{(\mathrm{I})})/(1+\varepsilon_0)$, respectively. In region I, the hoop strain $\varepsilon_{\varphi(\mathrm{I})} = \varepsilon_{r(\mathrm{I})} = \varepsilon_0$ because of the uniform hydrostatic tension, while in region II it is no longer a constant, expressed by the cone angle θ as

$$\varepsilon_{\varphi(\mathrm{II})} = \frac{R_g \sin\theta - r}{r} = \frac{\sin\theta(1+\varepsilon_0)}{\theta - \omega_{(\mathrm{I})} + \sin\omega_{(\mathrm{I})}} - 1 \quad \left(\omega_{(\mathrm{I})} \le \theta \le \omega_s\right). \tag{2}$$

In region III, the graphene sheet accords perfectly with plane stress problems, and thus the Lame Solution can be applied directly to this region. Using the hoop strain continuity at $r = r_{(\mathrm{II})}$, the strains in region III can be obtained as

$$\varepsilon_{r(\mathrm{III})} = -\frac{(1+\nu)r_g^2/r^2 - (1-\nu)}{(1+\nu)r_g^2/r_{(\mathrm{II})}^2 + (1-\nu)} \times \left[\frac{\sin\omega_s(1+\varepsilon_0)}{\omega_s - \omega_{(\mathrm{I})} + \sin\omega_{(\mathrm{I})}} - 1\right] \quad (r_{(\mathrm{I})} \le r \le r_{(\mathrm{II})}), \tag{3}$$

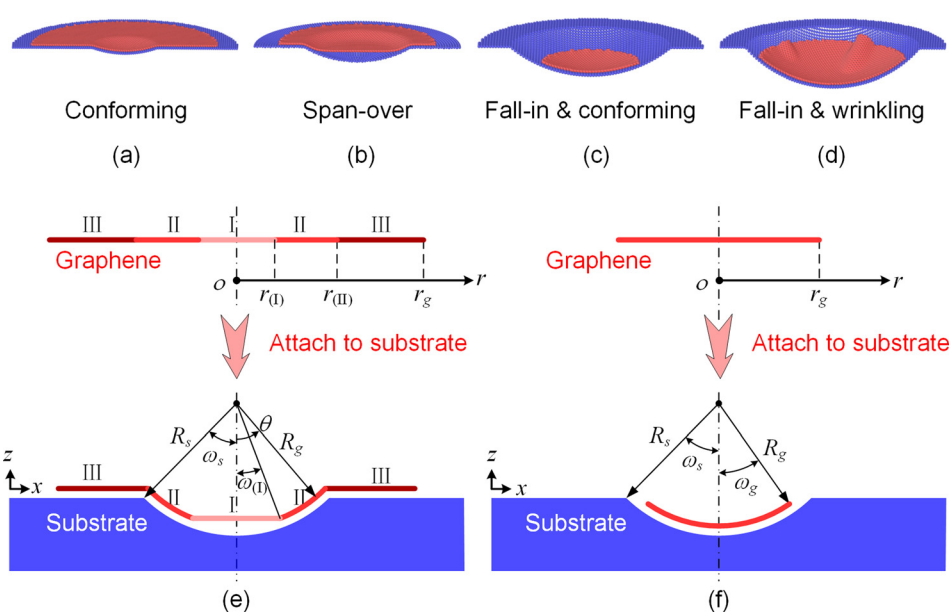

FIG. 2. Four types of final graphene morphology, (a) completely conforming to the substrate, (b) spanning over the substrate, (c) inside the concave and conforming, and (d) inside the concave and wrinkling, and two theoretical models for morphology prediction, (e) the model for relatively large graphene sheet: $\omega_{(\mathrm{I})} = 0$ indicates type (a) of the morphology and $\omega_{(\mathrm{I})} > 0$ corresponds to type (b), and (f) the model for relatively small graphene sheet to predict types (c) and (d).

$$\varepsilon_{\varphi(\mathrm{III})} = \frac{(1+\nu)r_g^2/r^2 + (1-\nu)}{(1+\nu)r_g^2/r_{(\mathrm{II})}^2 + (1-\nu)} \times \left[\frac{\sin\omega_s(1+\varepsilon_0)}{\omega_s - \omega_{(\mathrm{I})} + \sin\omega_{(\mathrm{I})}} - 1\right] \quad (r_{(\mathrm{I})} \le r \le r_{(\mathrm{II})}). \tag{4}$$

Therefore, the membrane energy of the graphene is obtained by summing the membrane energies of regions I, II, and III as

$$E_m(\omega_{(\mathrm{I})}, \varepsilon_0) = \frac{\pi R_g^2 E t \varepsilon_0^2 \sin^2\omega_{(\mathrm{I})}}{(1-\nu)} + \frac{\pi R_g^2 E t}{1-\nu^2} \times \int_{\omega_{(\mathrm{I})}}^{\omega_s} \left(\varepsilon_0^2 + 2\nu\varepsilon_0\varepsilon_{\varphi(\mathrm{II})} + \varepsilon_{\varphi(\mathrm{II})}^2\right)\sin\theta \mathrm{d}\theta + \frac{\pi E t r_{(\mathrm{II})}^2\left(r_g^2 - r_{(\mathrm{II})}^2\right)}{(1+\nu)r_g^2 + (1-\nu)r_{(\mathrm{II})}^2} \times \left[\frac{\sin\omega_s(1+\varepsilon_0)}{\omega_s - \omega_{(\mathrm{I})} + \sin\omega_{(\mathrm{I})}} - 1\right]^2. \tag{5}$$

The bending energy of the graphene sheet can be written as

$$E_b = \int_{A_g} [2B_M(C_M - C_0/2)^2 + B_G C_G]\mathrm{d}A_g, \tag{6}$$

in which $B_M = 1.45\,\mathrm{eV}$ and $B_G = -1.1\,\mathrm{eV}$ are the bending rigidity and the Gaussian bending stiffness of monolayer graphene sheet, respectively.[32] $C_M = (k_1 + k_2)/2$ and $C_G = k_1 k_2$ are the mean curvature and the Gaussian curvature, respectively, where k_1 and k_2 are the two principal curvatures. C_0 is the spontaneous curvature and disappears for symmetrical surfaces.

In regions I and III, the principal curvatures k_1 and k_2 are both zero, and in region II they are both R_g^{-1}. Accordingly, the bending energy of graphene becomes

$$E_b(\omega_{(\mathrm{I})}) = 2\pi(\cos\omega_{(\mathrm{I})} - \cos\omega_s)(2B_M + B_G). \tag{7}$$

The adhesion energy between graphene and substrate can be given by

$$E_{ad} = \int_{A_g}\int_{A_s} V(d)\rho_s \mathrm{d}A_s \rho_g \mathrm{d}A_g. \tag{8}$$

Here, $\rho_g = 4/(3\sqrt{3}l_{C-C}^2)$ is the homogenized carbon atom area density, in which $l_{C-C} = 0.142\,\mathrm{nm}$ is the carbon-carbon bond length. A_s is the area of substrate and ρ_s is the homogenized area density of the top layer substrate atoms, because the interactions between lower layer atoms and graphene are very weak and can be ignored.[12,24] $V(d)$ describes the van der Waals (VDW) interactions between a carbon atom and a substrate atom with distance d, and can be estimated by the Lennard-Jones(L-J) 6–12 potential as

$$V(d) = 4\varepsilon\left[\left(\frac{\sigma}{d}\right)^{12} - \left(\frac{\sigma}{d}\right)^{6}\right], \tag{9}$$

where $\sqrt[6]{2}\sigma$ is the equilibrium distance and ε is the bond energy at the equilibrium distance. For the systems with monolayer graphene sheet and SiO_2 substrate, $\rho_s = 18.1\,\mathrm{nm}^{-2}$, $\varepsilon = 0.00513\,\mathrm{eV}$, and $\sigma = 0.293\,\mathrm{nm}$.[24,34]

For simplicity, the adhesion energy of region I can be ignored due to the large distance d. The graphene sheets in regions II and III are supposed to be perfectly conformed to the substrate with a constant distance h, then the area density of adhesion energy in regions II and III is estimated as[30,31]

$$\phi_{ad} = 2\pi\rho_g\rho_s\varepsilon\sigma^2\left(\frac{2\sigma^{10}}{5h^{10}} - \frac{\sigma^4}{h^4}\right) = -1.2\pi\rho_g\rho_s\varepsilon\sigma^2, \tag{10}$$

in which $h \approx \sigma$ is the equilibrium distance between graphene and substrate.[30,31] The adhesion energy is then obtained as

$$E_{ad}(\omega_{(\mathrm{I})}, \varepsilon_0) = \phi_{ad}\pi\left(r_g^2 - r_{(\mathrm{I})}^2\right) = -1.2\pi^2\rho_g\rho_s\varepsilon\sigma^2\left[r_g^2 - \frac{R_g^2\sin^2\omega_{(\mathrm{I})}}{(1+\varepsilon_0)^2}\right]. \tag{11}$$

The total energy of the graphene/substrate system is

$$E_T(\omega_{(\mathrm{I})}, \varepsilon_0) = E_m(\omega_{(\mathrm{I})}, \varepsilon_0) + E_b(\omega_{(\mathrm{I})}) + E_{ad}(\omega_{(\mathrm{I})}, \varepsilon_0). \tag{12}$$

Minimizing the total energy E_T by $\partial E_T(\omega_{(\mathrm{I})}, \varepsilon_0)/\partial\omega_{(\mathrm{I})} = 0$ and $\partial E_T(\omega_{(\mathrm{I})}, \varepsilon_0)/\partial\varepsilon_0 = 0$, the critical half cone angle $\omega_{(\mathrm{I})}$ of floating region and the radial strain ε_0 can be obtained. The critical half cone angle $\omega_{(\mathrm{I})}$ and the radial strain ε_0 can depict the equilibrium morphology of graphene sheet uniquely. If $\omega_{(\mathrm{I})} = 0$, the graphene sheet conforms completely to the substrate, otherwise the graphene sheet spans over the concave. Therefore, the critical condition between morphology types (a) and (b) is obtained and presented in Fig. 3 by the blue curve. If the size of graphene is much larger than the concave, i.e., the radius ratio $r_g/R_s \to \infty$, the type of graphene morphology depends only on the half cone angle of concave ω_s: the graphene sheet conforms completely to the substrate if $\omega_s \le 27.5°$ and spans over the concave if $\omega_s > 27.5°$.

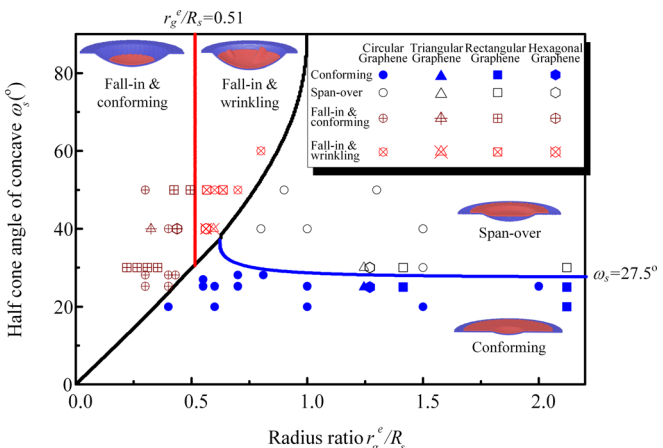

FIG. 3. The final morphologies of a monolayer graphene sheet with different shapes attached to the concave substrate. The solid lines are the critical conditions between different morphology types, obtained through theoretical analysis, and the scatters are results of MD simulations. For round graphene sheets, the equivalent radius r_g^e equals its radius r_g.

The above discussions are all based on the assumption that the graphene area is large enough to reach the flat edge of the concave, i.e., $r_g \geq R_g(\omega_s - \omega_{(\mathrm{I})} + \sin\omega_{(\mathrm{I})})/(1+\varepsilon_0)$, which is indicated by the black curve in Fig. 3. Otherwise, if $r_g < R_g(\omega_s - \omega_{(\mathrm{I})} + \sin\omega_{(\mathrm{I})})/(1+\varepsilon_0)$, the graphene sheet falls into the concave and morphology types (c) or (d) happens. In this case, the theoretical model in Fig. 2(f) is established for the critical condition between types (c) and (d). In this model, supposing that the sheet conforms to the concave completely, the membrane, bending, and adhesion energies are

$$E_m(r_g,\,\varepsilon_0) = \frac{\pi R_g^2 E t}{1-\nu^2}\int_0^{r_g(1+\varepsilon_0)/R_g}\left(\varepsilon_0^2 + 2\nu\varepsilon_0\left[\frac{\sin\theta(1+\varepsilon_0)-\theta}{\theta}\right] + \left[\frac{\sin\theta(1+\varepsilon_0)-\theta}{\theta}\right]^2\right)\sin\theta\mathrm{d}\theta, \tag{13}$$

$$E_b(r_g,\varepsilon_0) = 2\pi[1-\cos(r_g(1+\varepsilon_0)/R_g)](2B_M + B_G), \tag{14}$$

$$E_{ad}(r_g) = -1.2\pi^2\rho_g\rho_s\varepsilon\sigma^2 r_g^2. \tag{15}$$

The total energy of the graphene/substrate system is

$$E_T(r_g,\,\varepsilon_0) = E_m(r_g,\,\varepsilon_0) + E_b(r_g,\varepsilon_0) + E_{ad}(r_g), \tag{16}$$

in which ε_0 is the function of r_g and can be expressed by minimizing the total energy $\partial E_T/\partial\varepsilon_0 = 0$.

The critical condition between types (c) and (d) can be obtained by $\partial E_T/\partial r_g = 0$. The sheet conforms completely to the concave only if $\partial E_T/\partial r_g \geq 0$, and otherwise it wrinkles.[35] It is interesting to note that the critical condition between types (c) and (d) is determined only by the radius ratio r_g/R_s: the sheet conforms completely to the concave if $r_g/R_s \leq 0.51$ and wrinkles if $r_g/R_s > 0.51$, as shown in Fig. 3 by the red curve.

To verify the theoretical results, MD simulations are conducted by the large-scale atomic molecular massively parallel simulator (LAMMPS).[36] In all the simulations, the canonical ensemble (NVT) is adopted with temperature 300 K and time step is 1 fs. The SiO_2 substrate is fixed as a rigid body and the carbon-carbon bond interaction is described by the adaptive intermolecular reactive empirical bond order (AIREBO) potential[37] with the cutoff radius 0.192 nm.[38] The L-J potential in Eq. (9) is adopted to simulate the interactions between carbon atoms and substrate atoms with parameters $\varepsilon = 0.00513$ eV and $\sigma = 0.293$ nm.[24] In the simulations, appropriate disturbance is introduced by the restart instruction and the morphology of graphene is regarded as the final equilibrium state when the last restart simulation result has no difference from the former one. All four types of final morphology are investigated in the simulations and presented by different scatters in Fig. 3. It can be found that the theoretical prediction agrees well with the simulations results.

It should be noted that the above critical conditions are also applicable to monolayer graphene sheet with other shapes, although they are obtained from the circular graphene model for simplicity. For large graphene sheet, whether the graphene sheet conforms to or spans over the concave only depends on the half cone angle of the concave ω_s, which is independent of the graphene shape. In this case,

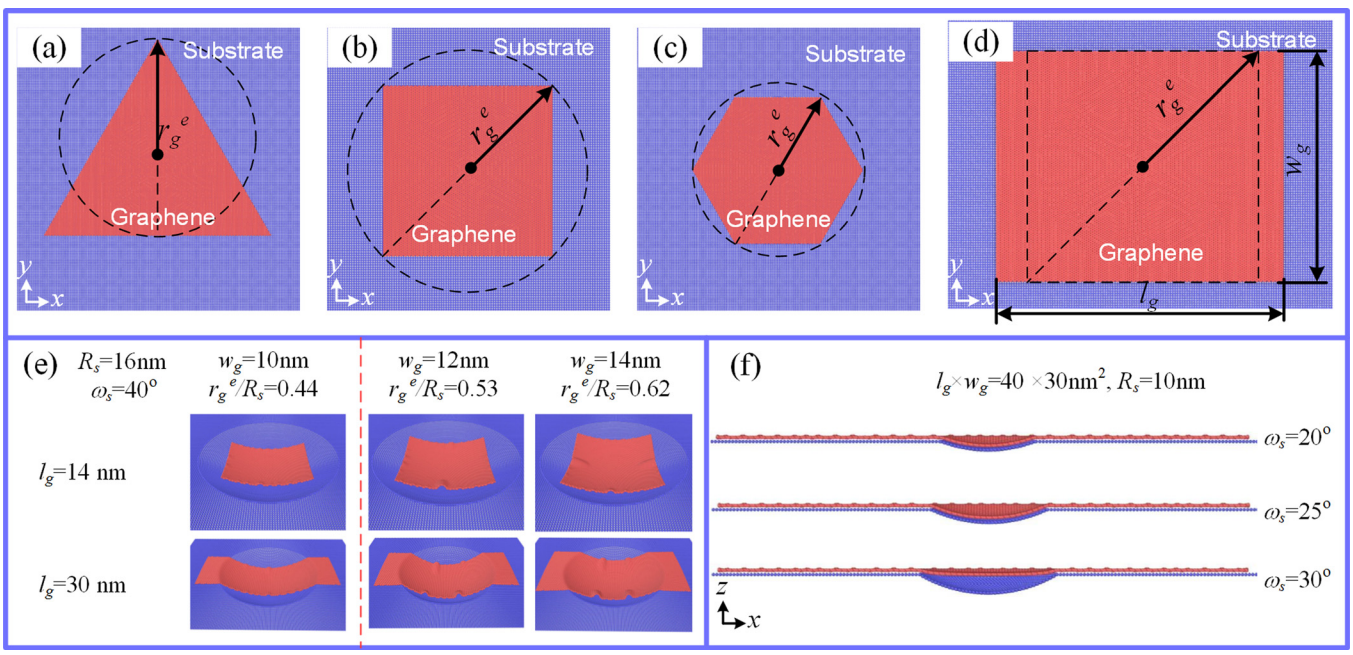

FIG. 4. The equivalent radius of (a) triangular, (b) square, (c) hexagonal, and (d) rectangular graphene sheets, and the morphologies of rectangular graphene sheets on the substrate with concave when the size of graphene sheet is (e) smaller and (f) much larger than the size of the concave.

MD simulations on triangular, rectangular, and hexagonal graphene sheets verify that the critical condition $\omega_s = 27.5°$ is still valid, as shown in Fig. 3. The morphologies of a rectangular graphene sheet are presented as an example in Fig. 4(f), in which the sheet fully conforms to the concave when $\omega_s = 25°$ and spans over the concave when $\omega_s = 30°$.

For small graphene sheet, the critical condition $r_g/R_s = 0.51$ can also be applied to graphene sheet with other shapes if a reasonable equivalent radius r_g^e is chosen to replace the radius r_g of circular graphene. According to MD simulation results, for regular polygon with edge number more than three, the circumradius can be used as the equivalent radius, as shown in Figs. 4(b) and 4(c), and the regular polygon with more edges is closer to the round shape. For triangular graphene sheet, half of the height is used as the equivalent radius, as illustrated in Fig. 4(a). The correlative MD simulations results are presented in Fig. 3 with different scatters. According to experimental observations, most of the graphene sheets are irregular and close to rectangle, and hence the rectangular graphene sheets are also studied. It is found that the appropriate equivalent radius for rectangular graphene sheet is the circumradius of the maximum square in the rectangle, as shown in Fig. 4(d), and Fig. 4(e) presents the simulation results of morphologies of rectangular graphene sheets, which indicates that the critical condition $r_g^e/R_s = 0.51$ is applicable.

The models and results of this letter can predict the graphene morphology on the substrate with concaves and decide whether or not the graphene sheet can conform completely to the substrate. Moreover, this work can be used to make active control on the graphene morphology. Conventionally, graphene sheets are desired to conform to the substrate without wrinkles so that their outstanding electronic and thermal properties can perform effectively. In these applications, including the ultimate chemical passivation protective coatings,[27] graphene-coated Si mold for precision glass optics,[28] and photovoltaic p–i–n thin film devices,[29] the concave half cone angle ω_s should be less than its critical value 27.5°. In some other applications, such as the graphene blister test[39] and graphene nanoelectromechanical switches,[40] the graphene sheet is required to span over the concave, and thus the concave half cone angle ω_s should be larger than 27.5°. It should be pointed out that the SiO_2 substrate is just an example to show the method and criterion between morphologies. The model and method in this work still hold for substrates with different adhesion parameters.

Support from the National Natural Science Foundation of China (Nos. 11202012 and 11472027) and the Program for New Century Excellent Talents in University (No. NCET-13-0021) is gratefully acknowledged.

[1]A. H. C. Neto, F. Guinea, N. M. R. Peres, K. S. Novoselov, and A. K. Geim, Rev. Mod. Phys. **81**, 109 (2009).
[2]D. Sánchez-Portal, E. Artacho, J. M. Soler, A. Rubio, and P. Ordejón, Phys. Rev. B **59**, 12678 (1999).
[3]M. Orlita, C. Faugeras, P. Plochocka, P. Neugebauer, G. Martinez, D. K. Maude, A. L. Barra, M. Sprinkle, C. Berger, and D. H. Wa, Phys. Rev. Lett. **101**, 267601 (2008).
[4]R. R. Nair, P. Blake, A. N. Grigorenko, K. S. Novoselov, T. J. Booth, T. Stauber, N. M. R. Peres, and A. K. Geim, Science **320**, 1308 (2008).
[5]S. Chen, Q. Li, Q. Zhang, Y. Qu, H. Ji, R. S. Ruoff, and W. Cai, Nanotechnol. **23**, 365701 (2012).
[6]F. Liu, P. Ming, and J. Li, Phys. Rev. B **76**, 064120 (2007).
[7]K. S. Kim, Y. Zhao, H. Jang, S. Y. Lee, J. M. Kim, K. S. Kim, J. H. Ahn, P. Kim, J. Y. Choi, and B. H. Hong, Nature **457**, 706 (2009).
[8]S. K. Lee, B. J. Kim, H. Jang, S. C. Yoon, C. Lee, B. H. Hong, J. A. Rogers, J. H. Cho, and J. H. Ahn, Nano. Lett. **11**, 4642 (2011).
[9]J. Liu, L. Cui, and D. Losic, Acta Biomater. **9**, 9243 (2013).
[10]W. Zhang, S. Lee, K. L. Mcnear, T. F. Chung, K. Lee, S. A. Crist, T. L. Ratliff, Z. Zhong, and Y. P. Chen, Sci. Rep. **4**, 795 (2014).
[11]J. Yoo, K. Balakrishnan, J. Huang, V. Meunier, B. G. Sumpter, A. Srivastava, M. Conway, A. L. Reddy, J. Yu, and R. Vajtai, Nano. Lett. **11**, 1423 (2011).
[12]S. Zhu and T. Li, J. Appl. Mech. **81**, 061008 (2014).
[13]J. Hicks, A. Tejeda, A. Taleb-Ibrahimi, M. S. Nevius, F. Wang, K. Shepperd, J. Palmer, F. Bertran, P. Le Fevre, J. Kunc, W. A. de Heer, C. Berger, and E. H. Conrad, Nat. Phys. **9**, 49 (2013).
[14]Y. Guo and W. Guo, J. Phys. Chem. C **117**, 692 (2013).
[15]Z. Zhang and T. Li, J. Appl. Phys. **107**, 103519 (2010).
[16]A. Fasolino, J. H. Los, and M. I. Katsnelson, Nat. Mater. **6**, 858 (2007).
[17]P. Süle, M. Szendrő, G. Z. Magda, C. Hwang, and L. Tapasztó, Nano. Lett. **15**, 8295 (2015).
[18]C. H. Lui, L. Liu, K. F. Mak, G. W. Flynn, and T. F. Heinz, Nature **462**, 339 (2009).
[19]V. Geringer, M. Liebmann, T. Echtermeyer, S. Runte, M. Schmidt, R. Rückamp, M. C. Lemme, and M. Morgenstern, Phys. Rev. Lett. **102**, 076102 (2009).
[20]T. Li and Z. Zhang, Nanoscale. Res. Lett. **5**, 169 (2010).
[21]T. Li and Z. Zhang, J. Phys. D: Appl. Phys. **43**, 075303 (2010).
[22]Z. H. Aitken and R. Huanga, J. Appl. Phys. **107**, 123531 (2010).
[23]H. Chen, Y. Yao, and S. Chen, J. Phys. D: Appl. Phys. **46**, 205303 (2013).
[24]Y. Zhou, Y. Chen, B. Liu, S. Wang, Z. Yang, and M. Hu, Carbon **84**, 263 (2015).
[25]H. C. Ko, M. P. Stoykovich, J. Song, V. Malyarchuk, W. M. Choi, C. J. Yu, J. B. Geddes, J. Xiao, S. Wang, Y. Huang, and J. A. Rogers, Nature **454**, 748 (2008).
[26]M. Lanza, T. Gao, Z. Yin, Y. Zhang, Z. Liu, Y. Tong, Z. Shen, and H. Duan, Nanoscale. **5**, 10816 (2013).
[27]E. Sutter, P. Albrecht, F. E. Camino, and P. Sutter, Carbon **48**, 4414 (2010).
[28]P. He, L. Li, J. Yu, W. Huang, Y. C. Yen, L. J. Lee, and A. Y. Yi, Opt. Lett. **38**, 2625 (2013).
[29]G. P. Veronese, M. Allegrezza, M. Canino, E. Centurioni, L. Ortolani, R. Rizzoli, V. Morandi, and C. Summonte, Sol. Energy Mater. Sol. Cells **138**, 35 (2015).
[30]L. Y. Jiang, Y. Huang, H. Jiang, G. Ravichandran, H. Gao, K. C. Hwang, and B. Liu, J. Mech. Phys. Solids. **54**, 2436 (2006).
[31]W. B. Lu, J. Wu, L. Y. Jiang, Y. Huang, K. C. Hwang, and B. Liu, Philos. Mag. **87**, 2221 (2007).
[32]Y. Wei, B. Wang, J. Wu, R. Yang, and M. L. Dunn, Nano. Lett. **13**, 26 (2013).
[33]A. Politano, A. R. Marino, D. Campi, D. Farias, R. Miranda, and G. Chiarello, Carbon **50**, 4903 (2012).
[34]M. Neek-Amal and F. M. Peeters, Phys. Rev. B **85**, 195445 (2012).
[35]C. Majidi and R. S. Fearing, Proc. R. Soc. London, Soc. A **464**, 1309 (2008).
[36]S. Plimpton, J. Comput. Phys. **117**, 1 (1995).
[37]S. J. Stuart, A. B. Tutein, and J. A. Harrison, J. Chem. Phys. **112**, 6472 (2000).
[38]T. Belytschko, S. P. Xiao, G. C. Schatz, and R. S. Ruoff, Phys. Rev. B **65**, 235430 (2002).
[39]N. G. Boddeti, S. P. Koening, R. Long, J. Xiao, and J. S. Bunch, J. Appl. Mech. **80**, 040909 (2013).
[40]X. Liu, J. W. Suk, N. G. Boddeti, C. Lauren, W. Luda, J. M. Gray, H. J. Hall, V. M. Bright, C. T. Rogers, M. L. Dunn, R. S. Ruoff, and J. S. Bunch, Adv. Mater. **26**, 1571 (2014).